Environment Canada

Water Science and Technology Directorate

Direction générale des sciences et de la technologie, eau

Environnement Canada

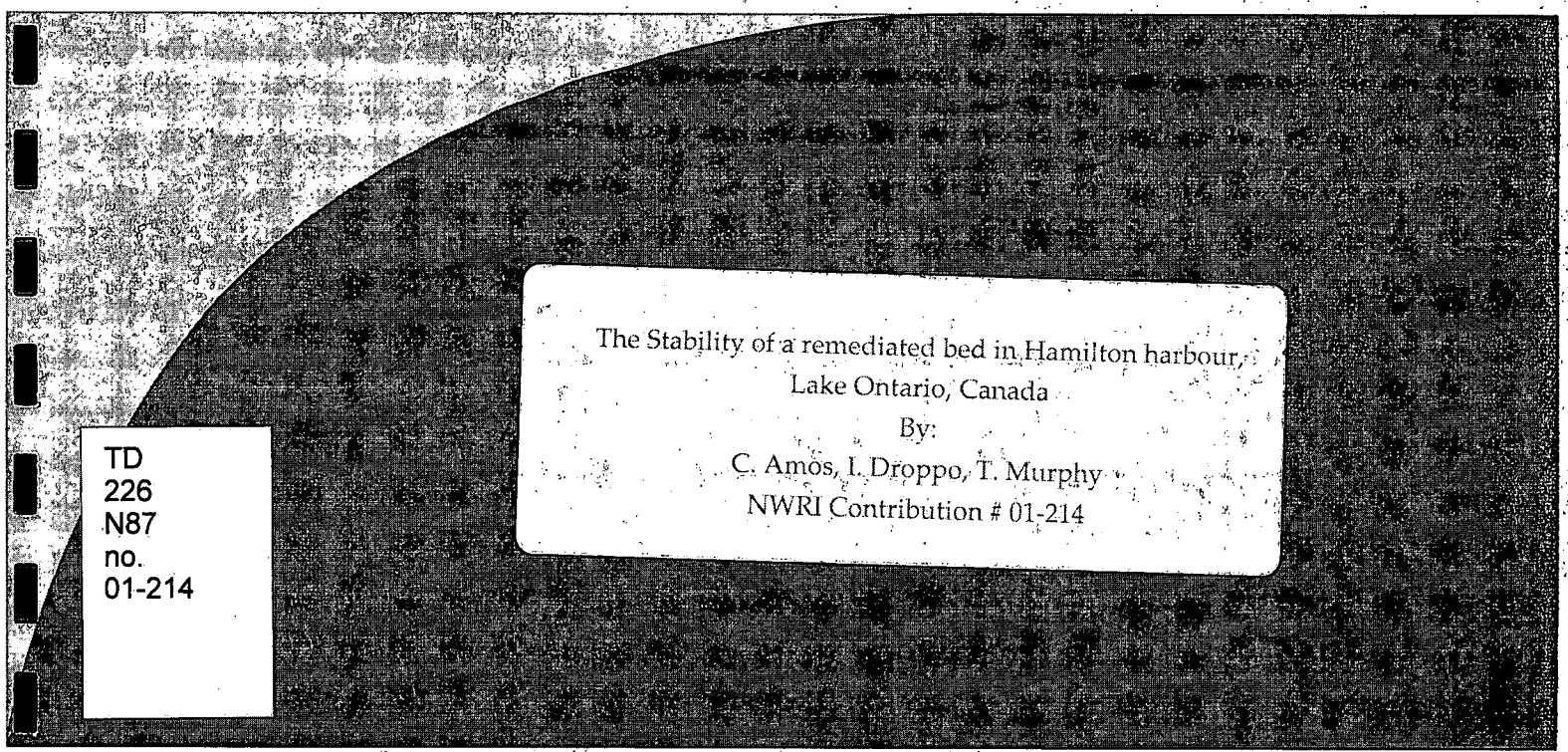

The Stability of a remediated bed in Hamilton harbour, Lake Ontario, Canada

By:

C. Amos, I. Droppo, T. Murphy

NWRI Contribution # 01-214

01-214

The stability of a remediated bed in Hamilton harbour, Lake Ontario, Canada

Carl L. Amos[1], Ian G. Droppo[2] and Tom Murphy[2]

NWRI Cont. # 01-214

[1] School of Ocean and Earth Science, Southampton Oceanography Centre, Southampton, Hampshire, UK, SO14 3ZH

[2] National Water Research Institute, P.O. Box 5050, Burlington, Ontario, CANADA

ACKNOWLEDGEMENTS

This project was considered a success due largely to the efforts of several key people. In particular we wish to thank: A. Robertson who helped mobilize and ship the GSCA Sediment Geodynamics container to Burlington; R. Murphy (GSCA) for technical support to CLA throughout the survey period; H. Don (NWRI) for boat handling a general field logistics while on site in Hamilton harbour; Dr B. Krishnappan (NWRI) for provision of the settling chamber and microscope used in the particle settling analyses; C. Jaskot for analyses of suspended sediments for IGD; and D. Clattenburg (GSCA) for the detailed grain size analyses. This project was funded by Environment Canada, and by RODAC funds to CLA.

Management Perspective

Many environmental contaminants have pathways that are partially or wholly associated with sediment and/or biological substrates. Consequently, on entering aquatic environments they find their way rapidly to the bed. An increase in bed shear stress can remobilize this material, with undesired effects on the aquatic environment. In situ remediation technologies are becoming increasingly popular for the "clean-up" of contaminated sediments. In this study, an *in situ* annular flume (Sea Carousel - Developed by C. Amos, Southampton Oceanography Center) was deployed in Hamilton Harbour, Lake Ontario, to investigate the impact of a remediation technology on contaminated sediment stability. Analysis was also made to assess the best method of determining the amount of energy required to initiate erosion (erosion threshold) and our freshwater results were compared to the more common marine erosion characteristics in the literature. Results, in support of the business line Nature, suggest that there appears to be no negative long-term impact of the remediation on the lakebed sediment stability. In fact there appears to be a strengthening with time over the natural bed, perhaps due to degassing during ploughing or increased bio stabilization. Erosion results were similar to those from salt water environments suggesting that salinity plays no direct role in controlling sediment erodibility. It is recommended that a regression extrapolation of suspended sediment concentrations and fluid transmitted bed shear stress to ambient concentrations be adopted for the evaluation of erosion threshold for future work.

Sommaire à l'intention de la direction

On observe, pour un grand nombre de contaminants environnementaux, des voies de transformation associées en partie ou en totalité à des sédiments et/ou à un substrat biologique. Pour cette raison, lorsque ces contaminants pénètrent dans le milieu aquatique, ils se retrouvent rapidement dans le lit du fond. Une augmentation de la contrainte de cisaillement du lit peut remobiliser ces matières, mais cela cause des effets non souhaitables sur l'environnement aquatique. Les technologies d'assainissement *in situ* deviennent de plus en plus populaires pour l'« assainissement » des sédiments contaminés. Pour cette étude, on a mis en place, dans le port de Hamilton (lac Ontario), un appareil à canal annulaire *in situ* Sea Carousel (mis au point par C. Amos, du Southampton Oceanography Center), afin d'étudier l'impact d'une technologie d'assainissement sur la stabilité des sédiments contaminés. On a aussi effectué des analyses afin d'évaluer la meilleure méthode pour déterminer la quantité d'énergie requise pour le déclenchement de l'érosion (valeur seuil d'érosion), et on a comparé les résultats obtenus avec des sédiments d'eau douce aux données sur l'érosion marine plus communes dans la documentation. Ces résultats, obtenus dans le cadre du secteur d'activité de la nature, semblent indiquer que l'assainissement des sédiments du lit n'a pas d'impact négatif à long terme sur leur stabilité. En fait, il semble y avoir un durcissement du lit naturel en fonction du temps, qui est peut-être dû au dégazage qui accompagne le labourage, ou à une biostabilisation accrue. Les valeurs d'érosion obtenues étaient semblables à celles des milieux marins, ce qui semble indiquer que la salinité ne joue pas de rôle direct dans la régulation des caractéristiques d'érosion des sédiments. Pour les prochaines études d'évaluation du seuil d'érosion, on recommande l'adoption d'une méthode d'extrapolation par régression des concentrations des sédiments en suspension et des contraintes de cisaillement du lit transmises par les liquides aux concentration ambiantes.

Stabilité d'un lit assaini dans le Port de Hamilton (lac Ontario, Canada)

Carl L. Amos[1)], Ian G. Droppo[2)] et Tom Murphy[2)]

I. School of Ocean and Earth Science, Oceanography Southampton Centre
Southampton, Hampshire, R.-U.
2) Institut national de recherche sur les eaux
C.P. 5050, Burlington (Ontario) CANADA

RÉSUMÉ

On a effectué, à trois sites du port de Hamilton, dans le lac Ontario, des mesures *in situ* de l'érodabilité des sédiments pour l'étude du milieu benthique dans le lit du lac, à l'aide de l'appareil à canal annulaire Sea Carousel. On a évalué trois méthodes d'estimation de la valeur seuil d'érosion en surface [$\tau_c(0)$] à l'aide d'une série chronologique de mesures effectuées avec le Sea Carousel : la première méthode applique une compensation par les moindres carrés aux mesures de résistance du lit par rapport à la profondeur du milieu érodé afin de dériver une valeur pour la surface, la seconde applique une régression à la vitesse moyenne d'érosion (E_m) en fonction de la contrainte de cisaillement du lit pour calculer la valeur seuil (résolution pour $E_m = 0$), et la troisième extrapole une régression des concentrations des sédiments en suspension (S) et des contraintes de cisaillement du lit transmises par les liquides (τ_0) afin d'obtenir des concentrations ambiantes. La première parcelle examinée, non perturbée (C), a servi de témoin; la deuxième (W) a été perturbée par le labourage et l'injection d'eau pendant le traitement du lit du lac, et la troisième, également perturbée, a reçu une injection d'oxydant pour l'assainissement des sédiments contaminés. Les principaux objectifs de cette étude étaient : 1) évaluer trois méthodes différentes possibles pour la dérivation de seuils d'érosion; 2) comparer les seuils d'érosion lacustres avec leurs homologues des estuaires marins et 3) examiner les effets du labourage et de l'utilisation d'amendements chimiques sur la stabilité du lit.

On a déployé cinq Sea Carousel dans la parcelle d'essai. Les valeurs moyenne du seuil d'érosion étaient : $\tau_{crit} = 0{,}52(\pm 0{,}06)$, $0{,}27(\pm 0{,}01)$ et $0{,}34(\pm 0{,}03)$ Pa pour les trois expériences extrapolées, respectivement. La méthode 1) prévoyait des résistances de lit trop élevées, étant donné qu'elle était fortement subjective et insensible aux effets dans la couche superficielle de 1-2 mm. Les résultats de la méthode 2) présentaient une forte dispersion des données, et la définition de la vitesse d'érosion de base (E_0) était plutôt arbitraire. La méthode 3), qui donnait des résultats stables, reproductibles et objectifs, est recommandée pour l'évaluation de la valeur seuil d'érosion. Pour ces seuils, qui étaient assez bien corrélés avec la masse volumique apparente des sédiments, on observait les mêmes tendances que pour les sédiments marins prélevés dans des sites très différents. Les taux de sédimentation massiques, exprimés sous forme de constante de déclin de la teneur en S, étaient fortement liés à cette dernière et correspondaient aux valeurs des sédiments marins. En conclusion, on peut dire que, dans les exemples présentés, les différences de salinité avaient peu d'effets sur les taux de sédimentation massique.

On a noté des différences significatives marquées entre les sites labourés et les sites témoins soit pour la vitesse d'érosion, soit pour le coefficient de frottement (ϕ), ce qui permet de conclure que le rétablissement du lit après la perturbation est rapide (moins de 24 heures). On notait aussi un accroissement linéaire en fonction du temps de $\tau_c(0)$ après le labourage, avec un retour à la valeur moyenne des sites témoins en 3 jours ou moins. Le coefficient de frottement était réduit à zéro par le labourage (diagnostic de fluidisation), mais il croissait de façon linéaire avec le temps et remontait aux valeurs des sites témoins au cours d'une période prévue de 6 jours.

Sedimentology (2003) **50**, 149–168

The stability of a remediated bed in Hamilton Harbour, Lake Ontario, Canada

CARL L. AMOS*, IAN G. DROPPO†, EDUARDO A. GOMEZ‡ and TOM P. MURPHY†

*School of Ocean and Earth Science, Southampton Oceanography Centre, Southampton, Hampshire SO14 3ZH, UK (E-mail: cla8@soc.soton.ac.uk)
†National Water Research Institute, PO Box 5050, Burlington, Ontario, Canada
‡IADO, Bahia Blanca, Argentina

ABSTRACT

In situ measurements of lakebed sediment erodibility were made on three sites in Hamilton Harbour, Lake Ontario, using the benthic flume Sea Carousel. Three methods of estimating the surface erosion threshold ($\tau_c(0)$) from a Carousel time series were evaluated: the first method fits measures of bed strength to eroded depth (the failure envelope) and evaluates threshold as the surface intercept; the second method regresses mean erosion rate (E_m) with bed shear stress and solves for the floc erosion rate (E_f) to derive the threshold for $E_m = E_f = 1 \times 10^{-5}$ kg m^{-2} s^{-1}; the third method extrapolates a regression of suspended sediment concentration (S) and fluid transmitted bed shear stress (τ_0) to ambient concentrations. The first field site was undisturbed (C) and acted as a control; the second (W) was disturbed through ploughing and water injection as part of lakebed treatment, whereas the third site (OIP) was disturbed and injected with an oxidant used for remediation of contaminated sediment. The main objectives of this study were: (1) to evaluate the three different methods of deriving erosion threshold; (2) to compare the physical behaviour of lacustrine sediments with their marine estuarine counterparts; and (3) to examine the effects of ploughing and chemical treatment of contaminated sediment on bed stability. Five deployments of Sea Carousel were carried out at the control site. Mean erosion thresholds for the three methods were: $\tau_c(0) = 0{\cdot}5$ (±0·06), 0·27 (±0·01) and 0·34 (±0·03) Pa respectively. Method 1 overpredicted bed strength as it was insensitive to effects in the surface 1–2 mm, and the fit of the failure envelope was also highly subjective. Method 2 exhibited a wide scatter in the data (low correlation coefficients), and definition of the baseline erosion rate (E_f) is largely arbitrary in the literature. Method 3 yielded stable (high correlation coefficients), reproducible and objective results and is thus recommended for evaluation of the erosion threshold. The results of this method correlated well with sediment bulk density and followed the same trend as marine counterparts from widely varying sites. Mass settling rates, expressed as a decay constant, k, of $S(t)$, were strongly related to the maximum turbidity at the onset of settling (S_{max}) and were also in continuity with marine counterparts. Thus, it appears that differences in salinity had little effect on mass settling rates in the examples presented, and that biological activity dominated any effects normally attributable to changes in salinity. Bedload transport of eroded aggregates (2–4 mm in diameter) took place by rolling below a mean tangential flow velocity (U_y) of 0·32 ms^{-1} and by saltation at higher velocities. Mass transport as bedload was a maximum at $U_y = 0{\cdot}4$ ms^{-1}, although bedload never exceeded 1% of the suspended load. The proportion of material moving as bedload was greatest at the onset of erosion but decreased as flow competence increased.

Given the low bulk density and strength of the lakebed sediment, the presence of a bedload component is notable. Bedload transport over eroding cohesive substrates should be greater in estuaries, where both sediment density and strength are usually higher. Significant differences between the ploughed and control sites were apparent in both the erosion rate and the friction coefficient (ϕ), and suggest that bed recovery after disruption is rapid (< 24 h). $\tau_c(0)$ increased linearly with time after ploughing and recovered to the control mean value within 3 days. The friction coefficient was reduced to zero by ploughing (diagnostic of fluidization), but increased linearly with time, regaining control values within 6 days. No long-term reduction in bed strength due to remediation was apparent.

Keywords Erosion threshold, lacustrine sediments, benthic flume, mass settling rates, deposition threshold.

INTRODUCTION

Erosion threshold is often used as the index of bed stability in the study of cohesive/adhesive muddy sediments, and a variety of methods have been used to define this threshold. An evaluation of some of these methods is given by Sutherland *et al.* (1998a), who found large differences in results depending on the method used. In the present study, this work is expanded, and the differences in results are examined in three extrapolation methods used to define erosion threshold. The purpose of the present investigation is to define a robust and objective means of defining sediment erosion threshold from *in situ* measures of suspended sediment concentration (S) in order to evaluate changes in bed stability. Absolute accuracy is not claimed in this study because of the lack of a 'traceable standard' in the estimation of bed shear stress over naturally roughened surfaces (Gust & Muller, 1997) and uncertainties in the definition of 'erosion threshold' (Lavelle & Mofjeld, 1985; Sutherland *et al.*, 1998a; Houwing, 1999).

Bioremediation of contaminated sediments has been undertaken in Hamilton Harbour, Lake Ontario (Murphy *et al.*, 1995), and involves the physical disruption of the topmost 0·3 m of lakebed by a towed rake and the injection of fluidized oxidant (calcium nitrate) into the sediment. Although the effects of this treatment on the stability and mobility of the lakebed have not been evaluated specifically, previous treatments carried out in St Mary's River have been shown not to enhance mobility of the sediments (Murphy *et al.*, 1996) on the basis of sediment traps placed both upstream and downstream of the treatment site.

Several *in situ* measurements of bed stability have been made in the marine environment, but few measurements have been made in lakes. Within the Great Lakes, analogous trends to marine counterparts have been found in flocculation rate and floc diameter (Lick *et al.*, 1992), resuspension and transport mechanics (Lick *et al.*, 1994), resuspension rates and thresholds (Ziegler & Nisbet, 1994) and sediment mass balances incorporating settling rates (Cardenas *et al.*, 1995; Ziegler & Nisbet, 1995). These observations have been incorporated within the sophisticated sedimentation models of Gularte *et al.*, 1980), Lee *et al.* (1981) and Ziegler & Lick (1997). The present study builds on this work to: (1) define the stability of natural lakebed sediments and how these differ from estuarine counterparts; (2) define the behaviour of sediments through controlled erosion events; and (3) determine the impact of bioremediation on bed stability. The study was undertaken using the benthic, annular flume Sea Carousel (Amos *et al.*, 1992) on a treatment test site in Hamilton Harbour, Lake Ontario, Canada.

BACKGROUND

Hamilton Harbour is an industrial port for the steel manufacturing industry located at the western end of Lake Ontario (Fig. 1), which is a freshwater setting. The harbour has a mean and maximum depth of 13 and 24 m, respectively, and an area of 2150 ha. The harbour is the receiving water body for a watershed of 49 400 ha that drains the surrounding limestone/dolomite Niagara escarpment and is sheltered from strong currents and large waves, so the

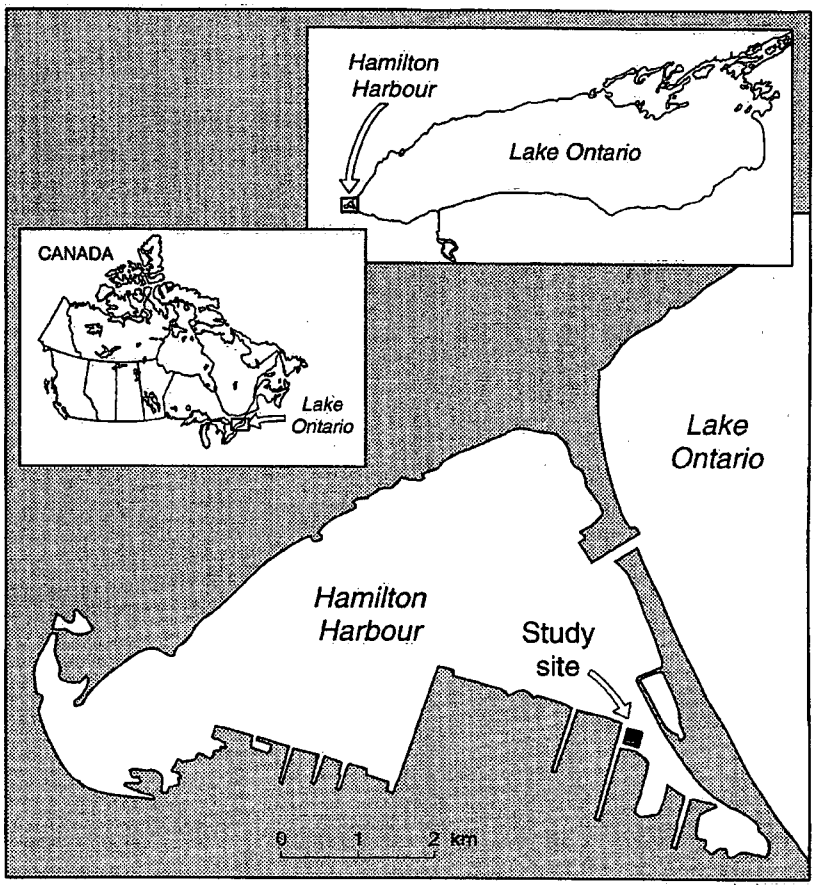

Fig. 1. Location diagram of Hamilton Harbour, situated at the western end of Lake Ontario, Canada.

site is depositional. The bed of the harbour is composed of 20 000 000 m^3 of gassy, organic-rich (7% dry weight), contaminated silt with a water content of 330% (Rukavina & Versteeg, 1996). Most of the contamination of the harbour (heavy metals, PCBs, PAHs, oil and grease) is the result of long-term storm-water runoff, sewer overflow, sewage treatment plant input, atmospheric input, direct overland flow and industrial input (Irvine *et al.*, 1998). The study site is situated ≈ 100 m off a steel plant in 5–7 m of water on a gently undulating, featureless lakebed (Fig. 1).

METHODS

Three adjacent test sites were marked out with Grimsby floats within a 50 × 50 m flat region of Hamilton Harbour. The first site was designated as control (C), the second (W) was ploughed and injected with lake water to a depth of 0·3 m, and the third (OIP) was ploughed and injected with calcium nitrate. The bed was ploughed by towing an 8 m wide injection rake over the lakebed in a manner described by Murphy *et al.* (1995).

A benthic flume (Sea Carousel) was used to carry out replicate *in situ* measurements of bed stability within the three sites. Sea Carousel is a benthic annular flume designed for field use in subaqueous settings and is 1·0 m in radius with an annulus 0·15 m wide and 0·30 m high. It weighs ≈ 40 kg in water, is made of aluminium (Fig. 2) and, by rotating a moveable lid that is driven by a 0·75 hp surface-powered digital stepping motor, it induces flow in the annulus. Eight small paddles, spaced equidistantly beneath the lid, induce a flow of water in the annulus. The Carousel is equipped with three optical backscatter sensors (OBSs; Downing, 1983) with two of these being located non-intrusively in the inner wall of the annulus at heights of 0·03 and 0·18 m above the base. The third OBS detects ambient suspended sediment concentration (S) outside the annulus. A water-sampling port is situated in the outer wall of the annulus at a height of 0·2 m and is used to calibrate the OBS sensors and to collect samples for physical, biological and chemical analysis.

Mean flow in the Carousel was determined from a relationship between azimuthal speed and lid

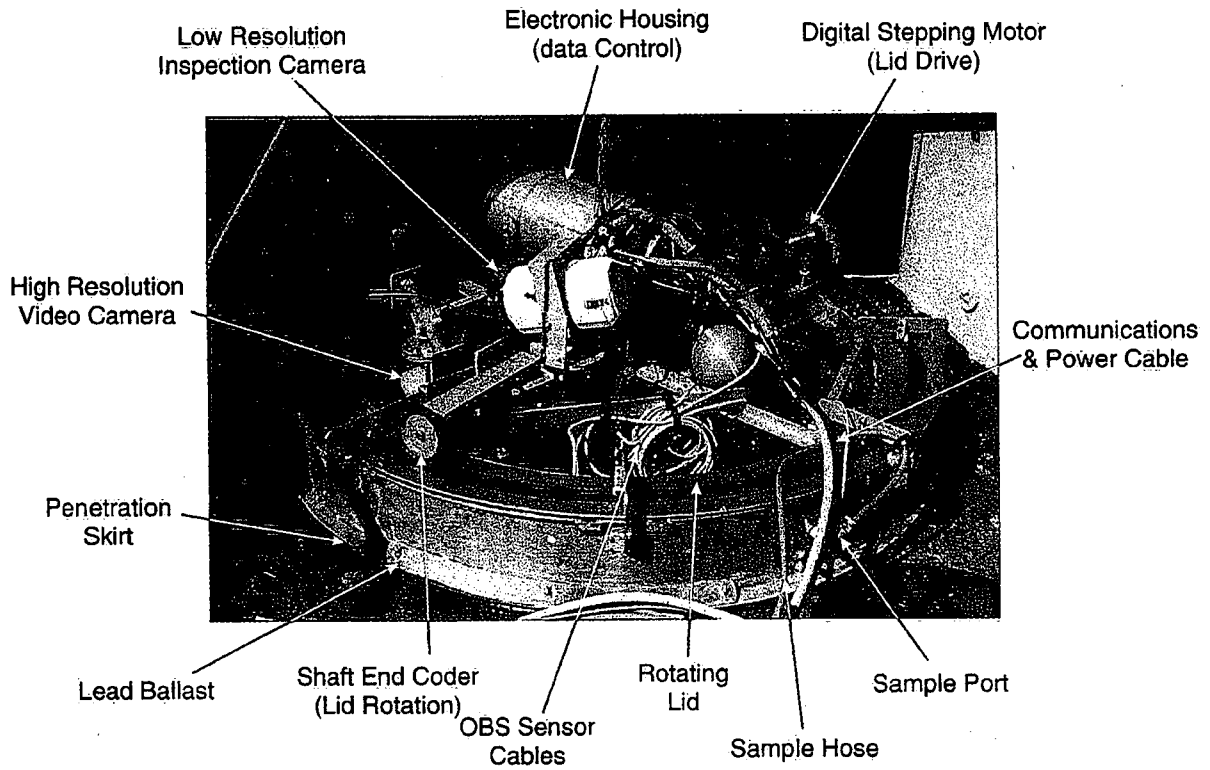

Fig. 2. Sea Carousel with the major equipment annotated.

rotation (Amos *et al.*, 1992) and was later verified in laboratory measurements using a variety of measurements (Thompson *et al.*, 2002). The mean tangential lid rotational speed was detected by a shaft encoder resting on the lid (Fig. 2), and the tangential (U) and vertical (W) mean current speeds were measured by a Marsh-McBirney® electromagnetic current meter (EMCM model 513–2·54 cm head diameter) situated ≈0·18 m above the bed. The current meter was calibrated in a tow tank at Bedford Institute of Oceanography and was accurate to ±20 mm s^{-1}. Electrical offsets in the EMCM depend on local conditions and so were determined *in situ* in still water at the start of each experiment. Output voltages from all sensors were digitized and transformed to absolute units in real time on a Campbell Scientific® CR10 data logger and stored on an SM192 storage module and a PC hard drive.

The sampling rate of all channels was 1 Hz, and flow speed was increased in steps through a series of script commands issued to the digital motor. The erosion process was recorded through a window in the side of the flume using a Sony® Handycam 8 mm video recorder held in an underwater housing. The bed was illuminated through a Perspex window by two 100-W lights powered from the surface. Pitch and roll sensors that were accurate to <1° monitored the flume attitude, while a Parascientific® pressure sensor measured flow depth from within the electronic housing to a resolution of ± 10 mm.

DEFINITIONS

Sea Carousel

The underlying assumption in the evaluation of bed response is that the detection sensors account for the total suspended mass (S) eroded from the bed in Sea Carousel; that is, continuity of this mass is maintained. Sediment continuity in three dimensions is given by:

$$\frac{\partial S}{\partial t} + \bar{U}\frac{\partial S}{\partial x} + \bar{V}\frac{\partial S}{\partial y} + \bar{W}\frac{\partial S}{\partial z} = 0 \qquad (1)$$

where the first term is the change in S with time, which is measured by the inside OBS sensors, and the last three terms represent tangential, radial and vertical advection by mean currents U, V and W in the x, y and z directions respectively.

Equation 1 is simplified within the closed environment of the Sea Carousel as the second and third terms are eliminated. The last term is

also simplified to a benthic flux resulting from the small depth within the flume (usually 0·3 m, but this varied depending on penetration of the flume into the bed) and assumes well-mixed conditions:

$$\frac{\partial S}{\partial t} - \bar{W}_s \bar{S} = 0 \qquad (2)$$

where W_s is the vertical mass velocity (in this notation, positive is downwards). Note that vertical diffusion through the water column, which is proportional to $\partial^2 S/\partial z$, is zero under the well-mixed conditions assumed here and so is ignored.

Leakage from the flume took place continuously across the moving lid. During periods of bed erosion, S in the flume was considerably greater than the ambient S, causing sediment losses. These losses were quantified using the diffusion equation of Sverdrup (1952) with a diffusivity constant (ε) of $1{\cdot}43 \times 10^{-3}$ m^2 s^{-1}; $\delta S/\delta x$ expresses the gradient in concentration across the flume wall ([(OBS1 + OBS3)/2)–OBS2]/Δy), where Δy was evaluated from independent experiments on dispersion (Amos *et al.*, 1992):

$$h\frac{\partial S}{\partial t} = -\bar{W}_s \bar{S} + \varepsilon \frac{\partial S}{\partial \Delta y} \qquad (3)$$

where h is the flume flow depth. The depth of erosion (z) beneath the flume was determined using Exner's formula:

$$\rho_b(1-P)\frac{\partial z}{\partial t} = h\frac{\partial S}{\partial t} = -\bar{W}_s \bar{S} + \varepsilon \frac{\partial S}{\partial \Delta y} \qquad (4)$$

The depth of erosion (from McDowell & O'Connor, 1977) was derived from the sum of the changes in S (measured), leakage (estimated) and the benthic flux (derived) where P is the sediment porosity, and ρ_s is sediment density. In a well-mixed case, the buoyant (upward) flux is equated with the benthic flux, where the benthic flux is the difference between the deposition (D) and erosion (E) rates:

$$\bar{W}_s \bar{S} = D - E \qquad (5)$$

It is assumed that, when $E > 0$, then $D = 0$ and, when $D > 0$, then $E = 0$: Partheniades *et al.* (1968) and Lau & Krishnappan (1994) have verified this assumption. Assumptions made in estimating eroded depth (z) are: (1) the sediment bulk density profiles derived from CT scanner analysis of cores are representative of the Sea Carousel site as they were adjacent to each other; (2) the density profile is constant over the footprint of the Sea Carousel; and (3) erosion is constant within the flume.

The time series of the erosion process may be transformed into a depth profile of sediment yield strength ($\tau_b(z)$) to create a synthetic core. This is based on the assumption that, at the point at which erosion ceases, within each increment of flow $\tau_0 = \tau_c(z) = \tau_b(z)$. Thus, by plotting the applied bed shear stress vs. eroded depth and fitting lines to the data trends, structure within the lakebed sediments begins to emerge. The trends in strength with depth can be quantified in terms of the friction coefficient, which is defined below.

The effect of S on the suppression of bed shear stress is complex because of: (1) turbulence dampening resulting from changes in the Monin–Obhukhov length scale (the ratio of turbulent kinetic energy production by shear to energy consumption by sediment mixing): Bagnold (1966), Best & Leeder (1993), Crapper & Ali (1997), Li & Gust (2000) and Baas & Best (2002) have examined this effect; (2) changes in viscosity of the fluid with consequent effects on the structure of the viscous sublayer (Gust, 1976); and (3) fluid momentum transfer to accelerating saltating aggregates brought into suspension during the erosion process (Bagnold, 1936; Amos *et al.*, 2000). Notwithstanding the above, experiments on stress reduction are inconclusive because of the lack of a traceable standard of bed shear stress over naturally roughened beds. Nevertheless, the following stress reduction algorithm has been applied to the present data on the basis of results in Amos *et al.* (1992) and Li & Gust (2000):

$$U_s^* = U^* - \{0{\cdot}2267[\log_{10}(S)].(U^*/6{\cdot}35)\}\ \mathrm{cm\,s^{-1}} \qquad (6)$$

where S is evaluated in mg L^{-1} and clear-water friction velocity $U^* = \sqrt{(\tau_0/\rho)}$ and U_s^* is the turbidity-reduced friction velocity. τ_0 was evaluated using the quadratic stress law, where $\tau_0 = C_d \rho U^2$ and $C_d = 4{\cdot}0 \times 10^{-2}$ (Amos *et al.*, 1992). The mean azimuthal flow in the flume (U) was determined from mean lid rotational speed (R) using a laboratory-derived equation: $U = 0{\cdot}574(R)$; $r^2 = 0{\cdot}92$; lid rotation was checked routinely *in situ* by tracking marks on the rotating lid with video and was found to be constant. The mean mass settling rate is calculated from:

$$W_s = (\delta M/\delta t)/S(t) \qquad (7)$$

at 10 s intervals of t throughout the settling period, and W_s is transformed according to Gibbs

et al. (1971) into an equivalent sedimentation radius ($d/2$, in cm) by:

$$d/2 = P1 + \sqrt{P2 + [P5(P3 + P4)]}/P5 \quad (8)$$

where $P1 = 0{\cdot}055804(\rho^2_{Ws})$, $P2 = 0{\cdot}003114$ $(\rho^2{}_{Ws}{}^4)$, $P3 = 4{\cdot}5\mu W_s$, $P4 = 8{\cdot}704 \times 10^{-3}$ (ρ^2_{Ws}) and $P5 = 981(\rho_b - \rho)$, in which μ is the absolute viscosity of fresh water at 20 °C (0·0131 poises), ρ_b is the aggregate bulk density equated with the sediment bulk density at the equivalent eroded depth (all evaluated in cgs units). Stokes Law is not applicable to the fast settling sediments of this study (Middleton & Southard, 1984). The fluid density was adjusted for S as follows:

$$\rho = [\rho_o(1 - V_s) + \rho_s V_s] \quad (9)$$

where ρ_o is the clear-water density (1000 kg m^{-3}), V_s is the suspended sediment volume, and ρ_s is the sediment density (2650 kg m^{-3}).

Bed stability is defined in terms of four measurable characteristics:

(1) The erosion threshold (cohesion) ($\tau_c(0)$) is interpreted as the point at which the surface of the bed begins to erode and is defined in three ways in this study:

(a) Method 1: the surface intercept of the failure envelope on plots of applied shear stress vs. eroded depth. Such plots define changes in sediment strength throughout the erosion process and assume that, at an applied bed shear stress (τ_0), mean bed erosion (E_m) will stop at the time (t) when the bed has eroded to a depth (z) at which the bed strength (τ_b) equals the applied stress: $\tau_b(z) = \tau_c(z) = \tau_0(t)$ and $E_m = E_f$ (Mehta & Partheniades, 1982).

(b) Method 2: the value at which the erosion rate approaches a nominal erosion rate at zero shear ($E_f = 1 \times 10^{-5}$ kg m^{-2} s^{-1}) in a regression of erosion rate vs. applied bed shear stress.

(c) Method 3: the value at which sediment concentration, S, approaches ambient conditions (S_o) on a correlation plot of (S) vs. applied bed shear stress.

(2) The friction coefficient (ϕ) is adapted from Terzaghi & Peck (1967): $\phi = \tan^{-1}(\tau_c(z)/\sigma')$ and uses results from the synthetic cores. Depth is transformed to an effective stress (σ') or buoyant geostatic load from a knowledge of sediment (wet) bulk density (ρ_b): $\sigma' = (\rho_b - \rho)gz + P'$, where g is the gravitational constant and P' is the ambient pore pressure (unknown and so assumed to be zero). In this study, ϕ is defined as the rate of change in bed strength with eroded depth. The locus that describes this relationship is called 'the failure envelope'. The value of ρ_b was taken as the mean of the topmost 10 mm of the sediment column: $\rho_b(C) = 1150$ kg m^{-2}; $\rho_b(W) = 1250$ kg m^{-2}; $\rho_b(OIP) = 1250$ kg m^{-2}.

(3) The mean erosion rate, E_m, is a function of applied bed shear stress and eroded depth; it is defined as the difference between the starting and final S within any velocity increment: $E_m = \delta M/\delta t = (S(t) - S(t - \Delta t))V_{sc}/\Delta t\alpha$, where M is the eroded dry mass, V_{sc} is the Sea Carousel volume (0·218 m^3), α is the flume bed area (0·87 m^2) and Δt is the duration of the applied eroding bed shear stress (after Krone, 1962).

(4) The type of erosion is either asymptotically diminishing with time (type I) or constant (type II; after Villaret & Paulic, 1986). Type I erosion is characterized by the release of flocs and small pellets (surface erosion), and the mode of transport is largely in suspension; type II erosion occurs through the release of rip-up clasts and large (up to 8 mm) aggregates (mass or bulk erosion) often seen moving as bedload.

Bottom sediment sampling

Bottom sediment samples were collected using an NWRI box corer. The corer was 0·50 × 0·50 m in plan and 0·80 m in length. Two syringe cores (60 cm^3), a push core 10·2 cm in diameter and a bulk sample were collected from the undisturbed central parts of the corer. The syringe cores were frozen immediately by immersion in liquid nitrogen and kept frozen for the analyses of bulk density and microfabric using a GE® Hilite scanner (Amos *et al.*, 1996a). The push core was frozen slowly and stored in a frozen state. Bulk samples were collected and kept at ambient temperatures for analyses of water content, organic carbon content, chlorophyll *a* content and grain size.

Water sampling

Water samples were collected from a sampling port (mid-depth) about 60 s into each flow increment. Known, well-mixed volumes (V_l) of the samples were filtered through a Swinnex® system onto preweighed, Gelmann® glass-fibre filters to remove the suspended solids. S was determined from the gravimetric weight of the suspended load (W_g): $S = W_g/V_l$. Duplicate samples were collected for particulate organic carbon,

major ion and chlorophyll *a* analysis as well as for conventional optical microscopy for observations of particle structure (Liss *et al.*, 1996). These samples were also analysed for suspended particle (floc/aggregate) size using an Optimax V system. Settling velocity was measured as well, and aggregate density was determined using a Northern Exposure® image analysis system (Droppo *et al.*, 1997). Size spectra of eroded particles were measured using a Malvern® particle size analyser (series 2600C) on water samples pumped from the Sea Carousel. Analyses of chlorophyll *a* and organic carbon were conducted according to the methods described by Parsons *et al.* (1984).

RESULTS

Bottom sediment analysis

The surface sediment texture was consistent, comprising between 10% and 15% sand, 43% silt with the remainder being clay. The disaggregated median diameter was 4–6 μm. The clay fraction was composed of illite, Fe-rich chlorite, an abundance of quartz, small amounts of smectite, vermiculite and traces of kaolinite (Murdoch & Zeman, 1975). The sediments were poorly sorted, reflecting a variety of sources. The sand fraction was largely made up of anthropogenic fly ash and other airborne industrial emissions. Analysis of major elements (EDAX) with time in the Sea Carousel showed that only SiO_2 varied throughout the deployment, systematically increasing in proportion to S. All other major ions (K, Cl, Na, Mg and SO_4) remained steady, reflecting an association with porewater fluids rather than siliceous sediment (Amos & Droppo, 1996; Droppo & Amos, 2001).

Sea Carousel

A summary of the results obtained from all deployments and tentative interpretations are given in Table 1. Five successful deployments of the Sea Carousel were completed at the control site (C2 was abandoned as the flume dropped into the sediments too rapidly causing unacceptable disturbance) and four in each of the disturbed

Table 1. Sea Carousel station summary including data on surface erosion thresholds (correlation coefficients given in brackets), computed friction coefficients and the range of wet weight sediment bulk densities determined from CT scanner analysis of syringe cores.

	Erosion threshold (Pa)				
Deployment site	Method 1 Eroded depth*	Method 2 Mean E†	Method 3 Mean S‡	Friction coeff. (ϕ) (degrees)	Bulk density (kg m^{-3})
C1	0·6	0·29 (0·73)	0·32 (0·93)	9	–
C3	0·5	0·28 (0·61)	0·32 (0·95)	12	920–1380
C4	0·4	0·25 (0·52)	0·31 (0·93)	11	–
C5	0·5	0·28 (0·47)	0·36 (0·95)	18	–
C6	0·5	0·27 (0·60)	0·38 (0·95)	11	–
Mean	0·5 ± 0·06 Pa	0·27 ± 0·01 Pa	0·34 ± 0·03 Pa	12·2 ± 3·1	–
	–	$r^2 = 0·59$	$r^2 = 0·94$		
W1	0·5	0·13 (0·78)	0·17 (0·96)	2	–
W2	0·5	0·36 (0·61)	0·40 (0·96)	3	–
W3	0·4	0·19 (0·63)	0·28 (0·97)	5	–
W4	0·6	0·26 (0·36)	0·48 (0·95)	8	1100–1430
Mean	0·5 ± 0·07 Pa	0·23 ± 0·08 Pa	0·33 ± 0·12 Pa	4·5 ± 2·3	–
	–	$r^2 = 0·59$	$r^2 = 0·96$		
OIP1	0·3	0·12 (0.74)	0·17 (0.96)	2	–
OIP2	0·4	0·22 (0.71)	0·29 (0.96)	5	–
OIP3	0·4	0·21 (0.57)	0·30 (0.98)	6	–
OIP4	0·5	0·23 (0.59)	0·38 (0.97)	8	1100–1530
Mean	0·4 ± 0·07 Pa	0·19 ± 0·04 Pa	0·28 ± 0·07 Pa	5·2 ± 2·2	–
	–	$r^2 = 0·65$	$r^2 = 0·97$		

* Calculated from synthetic core plots as surface intercept of bed strength.
† Calculated with corrected (dispersion) erosion rate.
‡ Calculated from corrected S.

sites. A typical time series from station C4 from the control site is shown in Fig. 3. Lid speed was increased in a series of 11 equal steps to 1·7 ms^{-1} (U_y = 0·97 ms^{-1}). Fully turbulent conditions, evident as azimuthal flow fluctuations, occurred above 0·3 ms^{-1} (U_y = 0·17 ms^{-1}); above these velocities, the assumption of fully mixed conditions is appropriate. The EMCM flow sensor showed very large and erratic fluctuations, probably caused by the highly magnetized nature of the anthropogenic material from stack emissions and surface runoff, which would influence the EMCM sensor. Consequently, lid speed was used to derive bed shear stress. Increases in S with time denoted erosion, which followed a type I pattern (asymptotically decaying). The erosion rate was generally greatest at the onset of each velocity increment and declined thereafter. Peak erosion rate increased with increasing applied flow velocity. Results of the corrected uppermost OBS showed synchronized trends of increasing S with current speed in Fig. 3A (the lowermost OBS was usually buried and so was not used). The plot of S, uncorrected for dispersion (leakage), agrees reasonably well with the pumped samples (solid dots, Fig. 3B). Figure 3C illustrates the erosion rate time series determined from the changes in corrected S with time. The erosion process began with movement of the organic-rich detritus (type Ia), which then gave way to erosion of bed material (type Ib) that moved partly as surface creep and partly in suspension. The erosion threshold was based on the onset of type Ib erosion. Surface creep (bedload) infilled depressions in the bed to create a smoothed surface and took place before the onset of mass

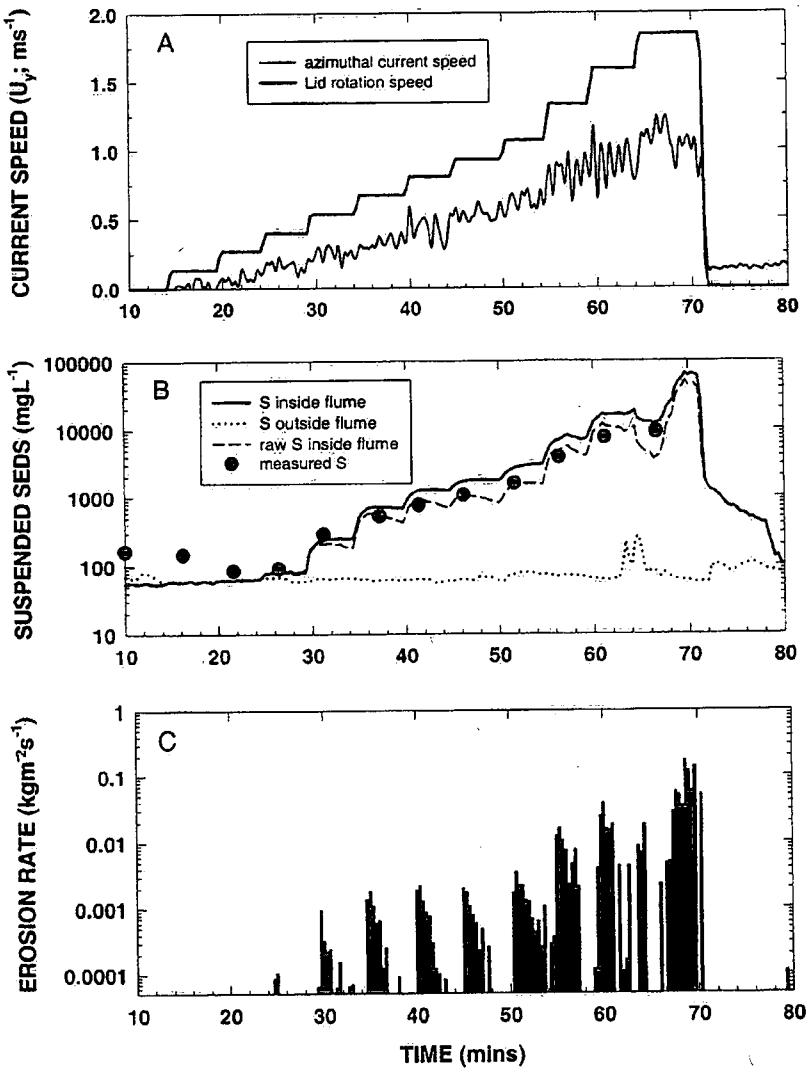

Fig. 3. Time series plot for control site C4. (A) Lid rotation and azimuthal current velocity. (B) Suspended sediment concentration (S) derived from gravimetric analysis and OBS sensors inside and outside the flume. (C) Erosion rates calculated from dispersion-corrected suspended sediment concentrations.

erosion of the bed. The mean size of aggregates moving as bedload was 2–3 mm and increased with mean velocity reaching maximum sizes of 10 mm. Bedload peaked at 0·3–0·4 ms^{-1} and dropped thereafter as aggregates moved into suspension. Above 0·3 ms^{-1}, saltation of aggregates began, which dominated the bedload component above 0·4 ms^{-1}. The finer fraction moved into suspension immediately, but suspension often lagged behind the onset of traction. Saltation of rip-up clasts was evident in all deployments. The mean frequency of aggregates through the field of view varied up to 3 s^{-1}.

Undisturbed site erosion thresholds and erosion rates

Examples of the three methods used to determine erosion threshold ($\tau_c(0)$) are shown in Fig. 4; all are taken from station C4. The erosion threshold ($\tau_c(0)$) in Fig. 4A is complicated by a change in ϕ at depths of 2 and 4·5 mm. The position of the

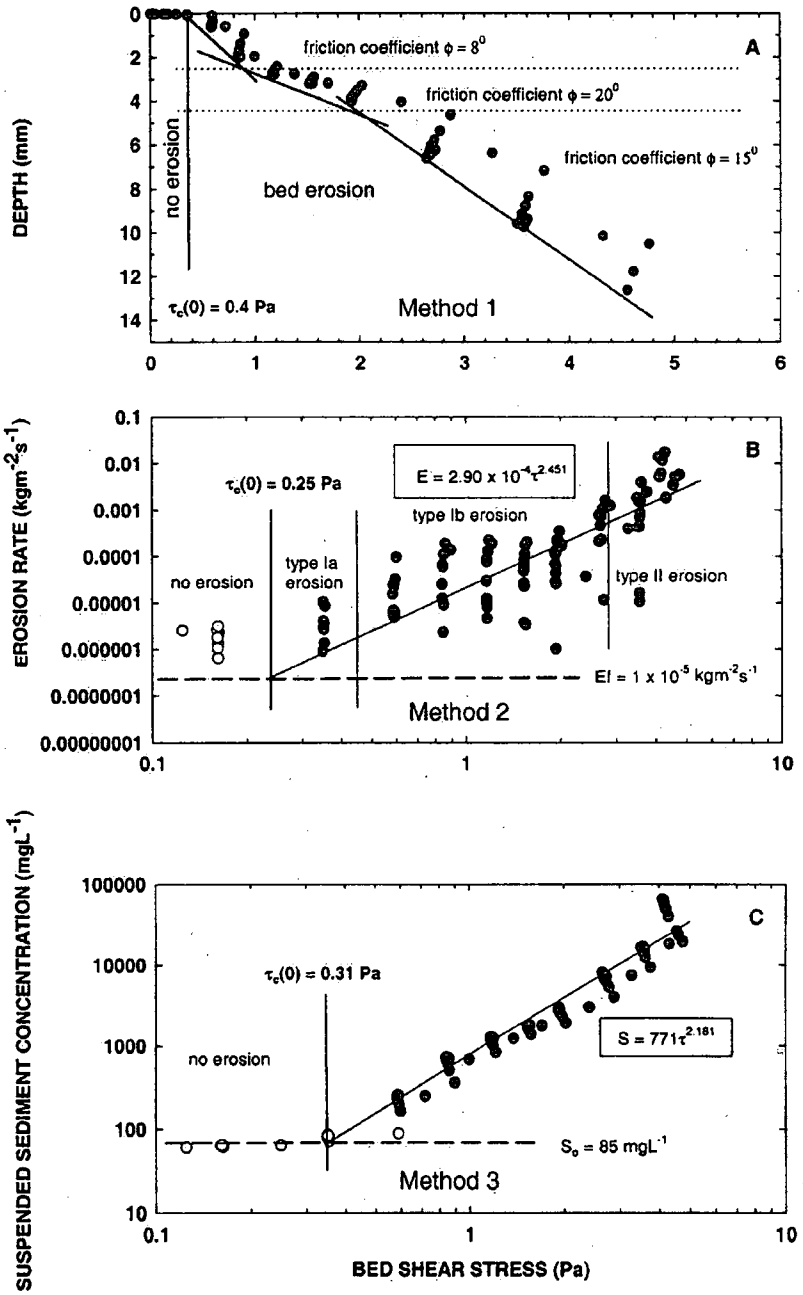

Fig. 4. Plots used in the determination of erosion threshold at control site C4. (A) Method 1: $\tau_c(0)$ is derived from the surface intercept of the failure envelope in the synthetic core plot. (B) Method 2: $\tau_c(0)$ is derived from regression of erosion rate on applied bed shear stress, solving shear stress for $E_m = 1 \times 10^{-5}$ kg m^{-2} s^{-1}. (C) Method 3: $\tau_c(0)$ is derived from regression of S on applied bed shear stress, solving for S at the ambient concentration.

failure envelop (joining points where erosion ceases) is subjective, thus reducing the reliability of the estimate of $\tau_c(0)$. The plot is, however, valuable in detailing the macrofabric of the sediment through changes in ϕ. This fabric is evident as three distinct layers of $\phi = 8°$, 20° and 15° with increasing depth. Method 2 is objective and reproducible (using regression analysis to derive $\tau_c(0)$). However, the low mean correlation coefficient ($r^2 = 0{\cdot}52$) reflects the uncertainty in the estimation of $\tau_c(0)$. Furthermore, extrapolation of the power function to an erosion rate of zero is not possible and so a 'background' rate (E_f) has been assigned a value of 1×10^{-5} kg m^{-2} s^{-1} (Parchure & Mehta, 1985). Method 3 is shown in Fig. 4C, where the correlation of data is stronger ($r^2 = 0{\cdot}93$), and the intercept (at ambient $S_o = 85$ mg L^{-1}) is unambiguous. A summary of $\tau_c(0)$ values is given in Table 1. The mean erosion thresholds for the control site for the three methods were: (1) 0·5 (±0·06) Pa; (2) 0·27 (±0·01) Pa, $r^2 = 0{\cdot}59$; and (3) 0·34 (±0·03) Pa, $r^2 = 0{\cdot}94$. The numbers in brackets define spatial heterogeneity and errors, which account for about 10% of the signal. Method 1 gave the highest scatter in results, and method 2 yielded the lowest. Methods 2 and 3 predicted substantially lower thresholds than method 1. Method 3 was reproducible and objective (yielding the highest r^2 values) and is considered to be the most reliable in this study. For purposes of comparison, this method was chosen as the standard.

Undisturbed site settling rates and size spectra

The mean still water mass deposition rate ($\delta M/\delta t$) has been derived from the rate of change in S within the Sea Carousel (after Krone, 1962; Einstein & Krone, 1967). The mean settling curves for the three sites (Fig. 5A) show an exponential

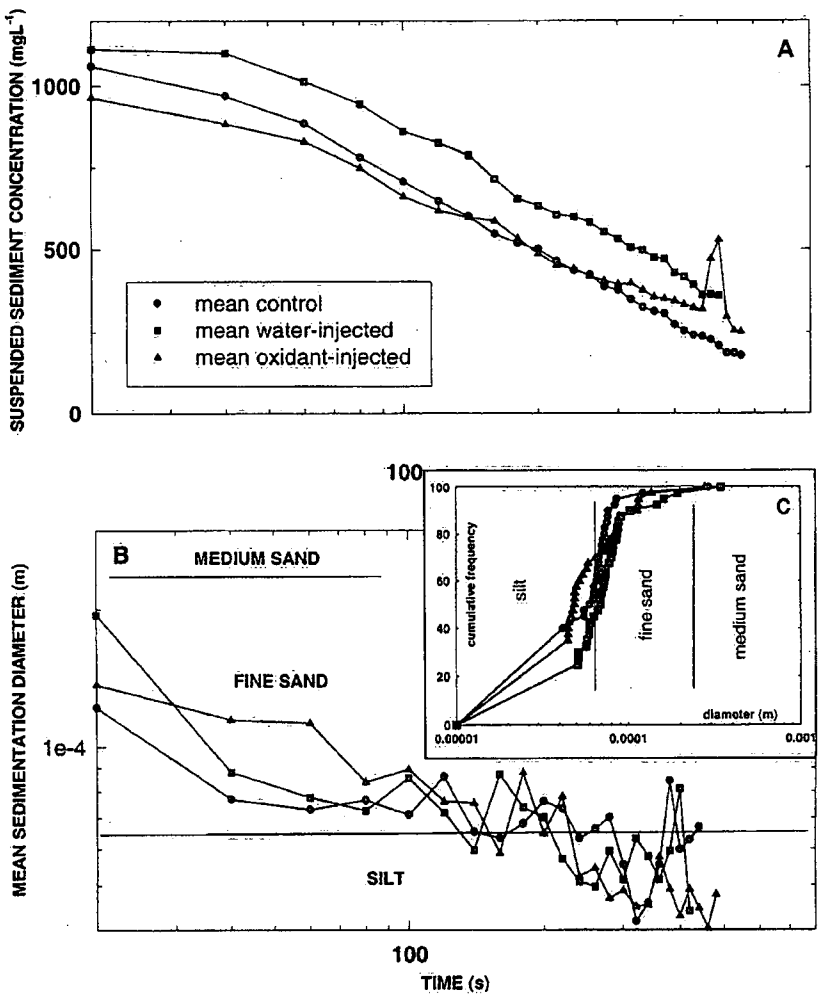

Fig. 5. Results of the still water settling for the three sites, illustrating (A) exponential trend in S with time, (B) fining in mean sedimentation diameter from fine sand to coarse silt with time, and (C) cumulative frequency distributions of the mean sedimentation diameters (d_s) for the suspended material determined from still water time series undertaken at the end of each erosion experiment.

decay in S with time. The computed mean values of mass settling rate (W_s) and equivalent sedimentation diameter (d_s) are presented in Table 2, and the latter are shown in Fig. 5B. Cumulative frequency distributions of the suspended material were derived from the settling time series. Site-averaged cumulative curves are shown in Fig. 5C. The control and water-injected sites show similar, narrow size spectra with 80% between 40 and 80 μm. The mean control d_s = 42 (±8) μm.

The still water-settling trend is expressed by the equation: $S(t) = -k\log_{10}(t) + b.W_s$ varied by a factor of three, whereas d_s varied from coarse silt (0·04 mm) to medium sand (0·37 mm). The mean decay constant in the settling equation varied as a function of the starting S_{max} and had the linear form: $k = 0{\cdot}35\ S_{max} - 14\ s^{-1}$ (Fig. 6). Both W_s and d_s varied throughout the settling period. The settling trend showed a decreasing settling rate with time. The equivalent sedimentation

Table 2. Calculated values of mass settling rate in terms of the decay constant (k) and mean particle settling rate (W_s); also shown is the mean sedimentation diameter (d_s) determined from W_s using the method described by Gibbs *et al.* (1971).

Deployment site	k (s^{-1})	S_{max} (mg L^{-1})	W_s (ms^{-1})	d_s (mm)
C1	−1100	2904	0·00064	0·040
C3	−653	1809	0·00094	0·040
C4	−1010	2615	0·00194	0·049
C5	−1029	2742	0·00183	0·051
C6	−661	1887	0·00131	0·027
Mean	890 (± 193)	2391 (± 453)	0·00133 (± 0·0005)	0·042 (± 0·008)
W1	−910	1304	0·00186	0·039
W2	−769	1733	0·00133	0·036
W3	−745	1373	0·00158	0·029
W4	−704	1128	0·00150	0·041
Mean	782 (± 77)	1384 (± 220)	0·00156 (± 0·0002)	0·036 (± 0·004)
OIP1	−736	1403	0·00180	0·064
OIP2	−743	1202	0·00121	0·034
OIP3	−779	1255	0·00151	0·036
OIP4	−583	1065	0·00130	0·047
Mean	710 (± 75)	1231 (± 121)	0·00145 (± 0·0002)	0·045 (± 0·011)

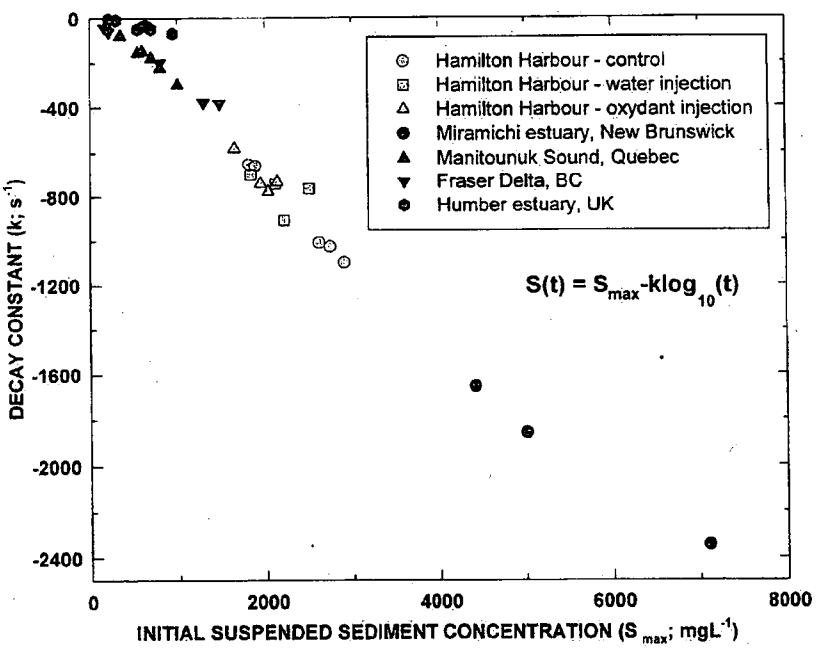

Fig. 6. The mean decay constant (k) of suspended mass in Hamilton Harbour as a function of maximum sediment concentration (S_{max}) at the onset of settling. A linear trend is evident, which is in continuity with previously published values of k from the marine environment. Notice that the trend is linear across a concentration range to 7000 mg L^{-1}, which suggests that free settling take place over this range.

diameters of the changing population of settling sediment varied from medium sand at the initial stages to coarse silt within the first 60 s of settling, which is considerably coarser than the disaggregated size population of 4–6 μm. Chlorophyll *a* showed a systematic increase from a background of 7 μg L^{-1} to maxima of over 200 μg L^{-1}. These increases were synoptic with *S*. Particulate organic carbon showed similar trends to *S* varying from 1 to 2 mg L^{-1} to over 200 mg L^{-1} as a result of bed erosion.

The effects of water injection

The time series plots did not appear to be significantly different from the control despite physical disturbance and fluidization of the sediment. Well-defined peaks in erosion rate (E_p) were evident at the onset of the first five increments of flow (above threshold), i.e. type I erosion. Thereafter, constant (type II) erosion prevailed under turbulent rough flow. The transition in erosion type took place at a lid speed of about 1 ms^{-1} (U_y = 0·57 ms^{-1}). The erosion threshold from method 1 was similar to that at the control site (0·5 ± 0·07 Pa). However, this threshold was well above those derived using methods 2 and 3 and supports the earlier finding that method 1 is a poor index of $\tau_c(0)$. The highly variable results are diagnostic of a spatially variable substrate, which may reflect disruption by the injection method. The mean erosion threshold derived from method 2 was 0·23 (±0·08) Pa, r^2 = 0·59, whereas that for method 3 was 0·33 (±0·12) Pa, r^2 = 0·96, which demonstrates a greater degree of site heterogeneity. The erosion thresholds at this site showed a systematic increase in strength with time. The site-averaged mean erosion rate (E_m) and *S* approximated a power relationship with bed shear stress. The friction coefficient was much less (4·5 ± 2·3) than at the control site and showed an increase with time.

The mass settling velocities were ≈20% higher than at the control site with a site-averaged value of 0·00156 (±0·0002) ms^{-1}. Mass settling velocities between sites were within the scatter and therefore trends could not be inferred. The site-averaged still water-settling rate was approximated by: $S(t) = -782 \log_{10}(t) + 2282$. The mean sedimentation diameter was 36 (± 4) μm and so was within the medium silt size range. W_s and d_s appeared to decrease throughout the period of settling, although considerable scatter was evident. The sedimentation diameters varied from fine sand during initial settling to coarse silt during the latter stages (Fig. 5B). The cumulative plot was similar to the control, indicating a similar size population of suspended aggregates.

The effects of oxidant injection

Time series plots were similar to those from the control and water injection sites. Erosion was dominated by type I erosion. The mean erosion thresholds for the three methods were 0·4 (±0·07) Pa, 0·19 (±0·04) Pa, r^2 = 0·65, and 0·28 (±0·07) Pa r^2 = 0·97. Results from methods 2 and 3 were about 30% less than those for the control. Friction coefficients (5·2 ± 2·2) were positive and showed monotonic increases with depth, diagnostic of a normal consolidation profile, as well as an increase with time (Table 1); however, these coefficient values were lower than the controls, indicating a reduction in strength. Erosion rates were power functions of applied stress and were similar in value to the control and water injection sites. The mean value of settling rate (W_s) was 0·00145 (±0·00023) ms^{-1} and was intermediate between the other sites. The median sedimentation diameter was 45 (±11) μm, which was not significantly different from the control. Chlorophyll *a* and POC showed values that overlapped those at the control and water injection sites.

DISCUSSION

Changes in bed stability with time

The period of this study was 17–25 August 1995. During this time, the air temperature exceeded 33 °C, and the water temperature was 25 °C. A relatively constant $\tau_c(0)$ = 0·34 Pa was apparent at the control site (Fig. 7A). However, significant changes were detected within the disrupted sites with no apparent differences between water and oxidant injection. The disrupted sites were ploughed completely twice about 6 h before the Sea Carousel deployment on 21 August. $\tau_c(0)$ shows minima immediately after ploughing (0·17 Pa) but, after 2 days, the bed strength had returned to the control mean value and, after 3 days, had exceeded the strength of the control (Fig. 7A). The bed strengthening appeared to be linear with time: $\tau_c(0,t) = 0{\cdot}16 + 0{\cdot}076(\Delta t)$, r^2 = 0·63. The friction coefficient showed similar trends (Fig. 7B); the control site ϕ was generally constant with time (12°), whereas the disrupted sites showed a reduction in ϕ to zero (fluidized)

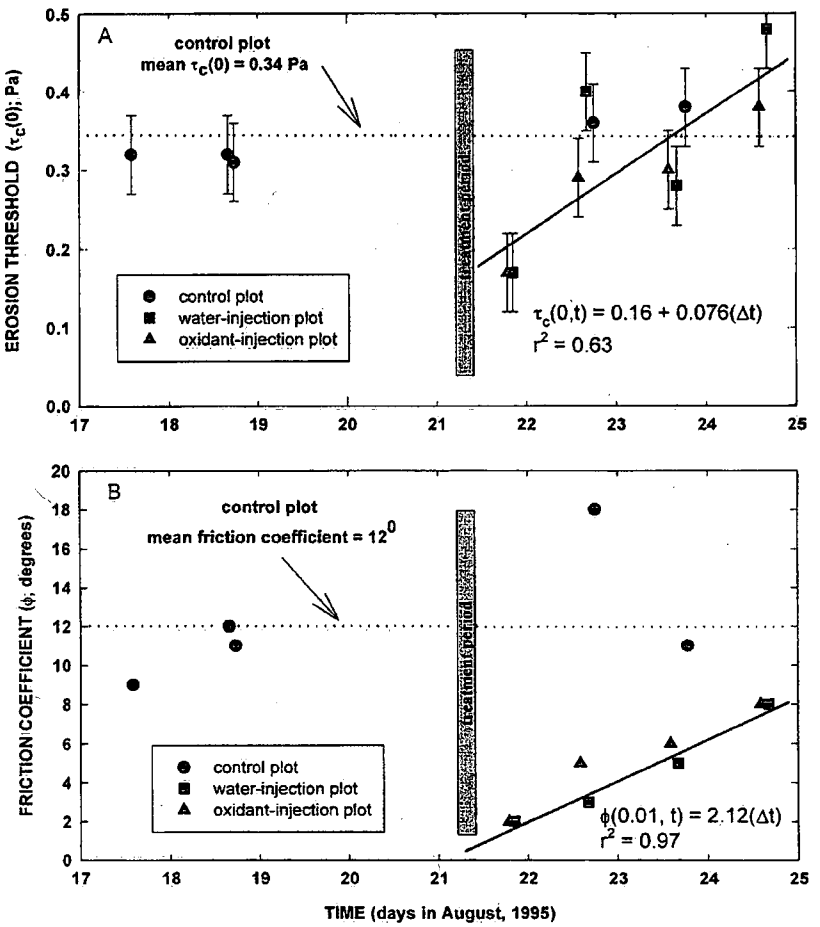

Fig. 7. Temporal changes in (A) erosion threshold and (B) friction coefficient for the three sites. The time series from the control site shows constant values, whereas the disturbed sites show initial weakening followed by systematic strengthening over 3 days.

and a linear increase with time after disruption with the form: $\phi(0{\cdot}01,\ t) = 2{\cdot}12(\Delta t)$; $r^2 = 0{\cdot}97$ (where 0·01 m is the depth of the estimation of ϕ). No differences were evident between the two disrupted sites, although there was a slight increase in chlorophyll *a* that may reflect the erosion of a developing biofilm.

Bed treatment appears to enhance stability, as is evident in increases in bed strength with time for both the erosion threshold and the internal friction coefficient. This effect is likely to increase with time because of the oxidation of organic matter, which bonds the sediment aggregates (Droppo & Amos, 2001). Oxidation, according to Murphy *et al.* (1996), is completed in about 6 days, whereas the present measurements spanned 3 days.

Comparison with marine settings

The erosion threshold (method 3) was compared with other values derived by Sea Carousel from Miramichi Bay, New Brunswick (Amos & Gibson, 1994), Lunenburg Bay, Nova Scotia (Sutherland, 1996; Sutherland *et al.*, 1998b), the Humber estuary, UK (Amos *et al.*, 1998a), Manitounuk Sound, Quebec (Amos *et al.*, 1996b), the Fraser River delta, British Columbia (Amos *et al.*, 1997), and Venice Lagoon, Italy (Amos *et al.*, 2000). All these examples are marine settings of varying salinities. Nevertheless, the erosion thresholds from these sites showed a positive trend with sediment wet bulk density (Fig. 8). The results from this study fall within the scatter of this trend and suggest that the freshwater sites behave similarly to the saline ones at similar bulk densities. The present results contrast sharply with those of Villaret & Paulic (1986), Williamson & Ockenden (1996) and Mitchener & Torfs (1996) that were conducted under laboratory conditions (see Lavelle *et al.*, 1984). Their results overlap those here within the region $1000 > \rho_b > 1400\ kg^{-3}$ but diverge at higher bed densities, with the laboratory results predicting much higher values. Cappucci (2002) monitored bed stability on intertidal mudflats in Venice Lagoon

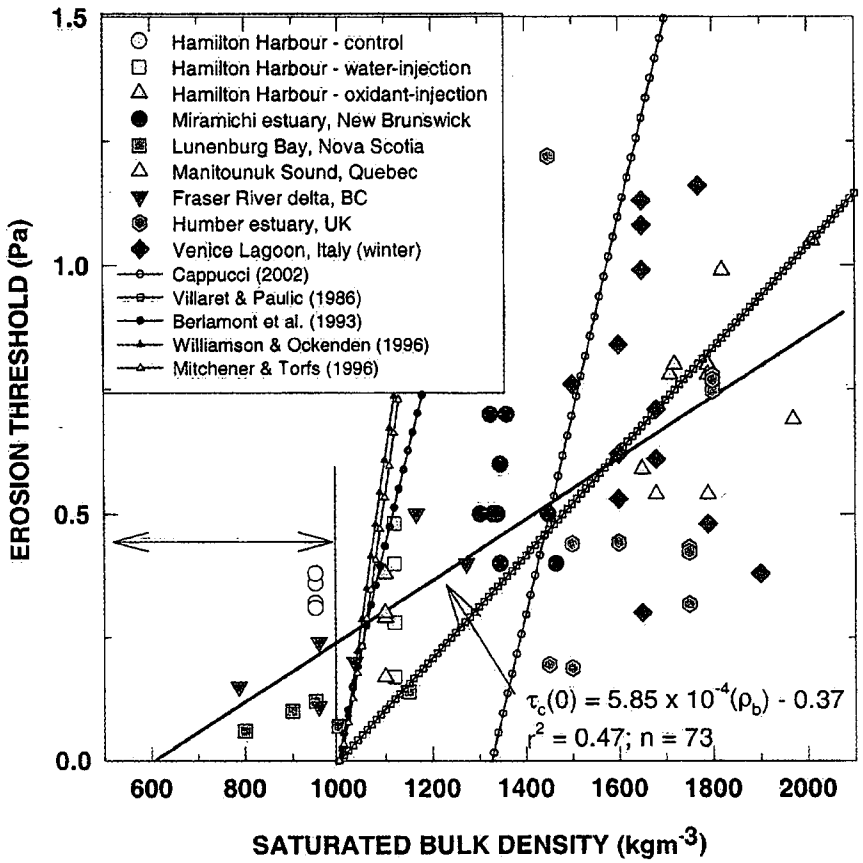

Fig. 8. The surface erosion thresholds measured in this study plotted against surface sediment wet bulk density based on CT scanner analyses of syringe cores taken at each site (Amos *et al.*, 1996a). The results follow a positive linear trend, which is in continuity with previously published examples from the marine environment and with those of Cappucci (2002). The near-surface sediment density in Hamilton Harbour was buoyant in places (arrow), indicating the presence of a lift force resulting from the presence of interstitial gas trapped within the structure of a surface biofilm (Droppo & Amos, 2001). The results of other laboratory studies are also shown for comparison: Villaret & Paulic (1986), Berlamont *et al.* (1993), Williamson & Ockenden (1996) and Mitchener & Torfs (1996).

using the cohesive strength meter of Paterson (1989) and showed trends similar to those described here, as did Tolhurst *et al.* (1997) using an impeller-type erosion device called EROMES.

The buoyant nature of the biofilm was observed by Sutherland *et al.* (1998b), who found buoyant, gassy bottom sediments within a mid-latitude microtidal estuary (Nova Scotia, Canada). Hamilton Harbour sediments are highly gas charged as a result of their anoxic state, and gas bubbles were observed to vent continuously from the bed throughout the erosion experiments. These bubbles create a lift force, which reduces the geostatic load (submerged weight). Once the sediment bulk density is lower than the density of water, the geostatic load is negative (lift), and the sediment is held in place by cohesive strength and biostabilization. The magnitude of the lift force/unit area is a measure of the upward-directed effective stress. For a 2 mm thick biofilm (evident in CT-scanned syringe cores) at the minimum density shown in Fig. 8 (950 kg^{-3}), the lift force is 0·98 Pa. This value is near the maximum strength of biostabilized sediments recorded by Sea Carousel shown in Fig. 8. The inference is that buoyant biofilms can be held in place by adhesion and organic binding to the bed provided that they are no thicker than 2 mm. Thicker buoyant biofilms would possess upward effective stresses larger than the biofilm strength and hence would break free and float to the surface. Within the context of this study, the lift force (F_l) per unit area acts to overcome the surface bed strength ($\tau_b(0)$). The 'true' critical shear stress for erosion ($\tau_c(0)$) is the addition of these two forces (per unit area):

$$\tau_c(0) = \tau_b(0) = F_l + \tau_0 \qquad (10)$$

Hence, the applied fluid bed shear stress (τ_0) at the onset of bed erosion is an 'apparent' critical value, which may represent only 30% of the true bed strength.

Buoyant aggregates have been observed in northern Venice Lagoon (Amos *et al.*, 1998b) in large quantities during periods of high temperatures and strong light and appear to contribute significantly to the sediment budget of the region. The bed of Hamilton Harbour is composed of a monoculture of Oligochaetes reflecting highly reducing conditions; the gas bubbles are thus probably caused by bacterial reduction and respiration.

The similarity in results of mass settling in still water between freshwater and marine sediments is dramatic and defined by $\partial S/\partial t = \overline{W_s S}/h_s = -k\,log(t)/\Delta t$. As t approaches unity, then $W_s = -kh_s/S$. As $-k$ is proportional to S (Fig. 6), then it follows that W_s is a function of the water depth at which S was measured (h_s) and thus independent of S. Thus, changes in W_s with time denote changes in sedimentation diameter, as evident in Fig. 5B. Figure 6 shows the decay constant for settling for four marine settings for $0 < S < 7000$ mg L^{-1}. The data from this study fit the linear trend over a range $1000 < S < 3000$ mg L^{-1} and are therefore in continuity with the marine examples. The inference of this is that salinity changes are unimportant to the process of mass settling of freshly eroded aggregates, such as those of the Sea Carousel, and that aggregate size is the important parameter.

Three methods have been used to monitor aggregate size: two direct measurements on pumped (disturbed?) samples and the third estimated as described earlier. The aggregates were analysed for the control site only during the erosion phases of C1, C3 and C5. Although not directly comparable, the assumption was made that the aggregates eroded from the bed during flow are those that settle during subsequent still water (neglecting corrasion). The results are plotted in Fig. 9. No trends were found in the median diameter (d_{50}) and sorting (vertical bars) through the erosion phase. The Malvern 2600C yielded values of $40 > d_{50} > 60$ μm, whereas the Optimax V showed a lower range of $20 > d_{50} > 50$ μm. The site-averaged median sedimentation diameters also show d_s to fall midway between the results of the two laboratory methods. Fennessy *et al.* (1997) found that the Malvern 2600C gave good results in settling experiments using an *in situ* settling column. However, as the two laboratory analyses were undertaken on the same samples, differences can only be the product of the instrument, sample preparation errors or a smaller sample population analysed by the Optimax V.

Bedload transport vs. suspended sediment transport

High-8 video observations made of the bed during the period of erosion show that eroded aggregates move initially as bedload (traction) followed by a

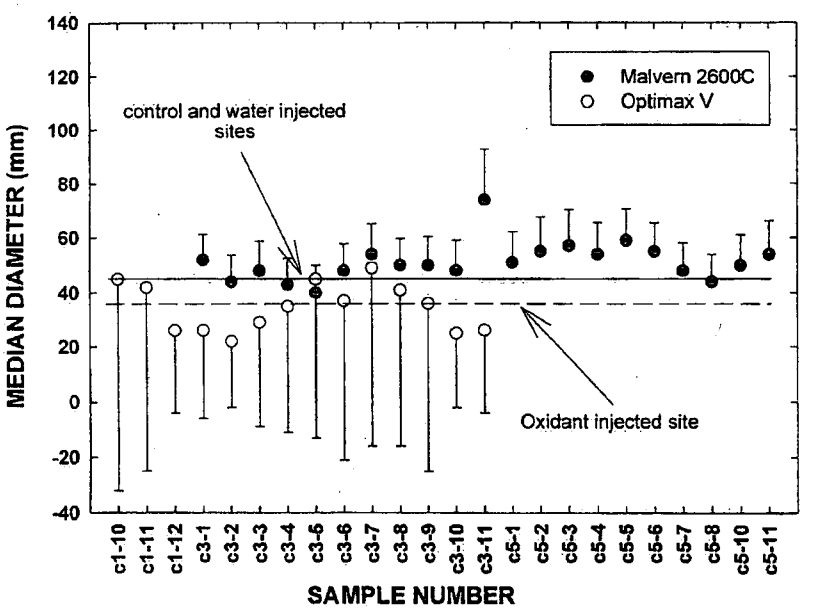

Fig. 9. The median aggregated diameter derived from pumped sample analyses using the Malvern 2600C and the Optimax V for increments of flow velocity during deployments C1, C3 and C5. These are compared with the sedimentation diameter (d_s) determined from still water-settling trends in S at the end of each *in situ* experiment. The results from the Malvern 2600C are larger than d_s, whereas the Optimax V results are lower. The two laboratory methods were undertaken on the same samples. Thus, the divergence in the results of the two laboratory methods results from sample preparation or instrument error.

period of saltation and then suspension. A full report on these analyses is given by Amos & Droppo (1996). The videos have been used to determine the mass fluxes and diameters of eroded aggregates in the three modes of transport (Fig. 10). Not all experiments are presented because of varying image quality. However, it is clear that aggregate motion as bedload is the first manifestation of the erosion process, and that this begins for $0{\cdot}15 > U > 0{\cdot}20$ ms^{-1}. The flux of aggregates in traction increases with current speed, and saltation begins for $U > 0{\cdot}3$ ms^{-1}. For $U > 0{\cdot}4$ ms^{-1}, the aggregates decrease in number as they move out of the field of view and into full suspension; for $U > 0{\cdot}5$ ms^{-1}, no aggregates are visible because of high turbidity. Using the bulk density values of the surface sediment (derived from the CT scanner) together with the measured mean diameters (2–4 mm), a dry mass transport rate is derived (Fig. 10B), which parallels the trends in aggregate numbers. There is a wide variation in results with no obvious clustering of the three experimental sites.

The suspended flux in the flume (Fig. 10C; $SUHw = 0{\cdot}045SU$, where H is flume height and w is flume width), shows a consistent trend with flow speed for all experimental sites, and the magnitude of the flux is several orders of magnitude larger than the bedload flux. The ratio of the suspended flux:bedload flux (Fig. 11) shows the highest value to be immediately after the onset of the erosion process, but it never exceeds 1%. The ratio decreases systematically with increasing current speed as more material is taken into suspension. The inference of the above is that the mechanism of erosion and mode of transport are strongly dependent on flow intensity: for intense events, suspension will dominate, whereas for weakly eroding events, bedload transport will probably play a major role in cohesive bed evolution.

Conclusions

A series of *in situ* measures of erodibility were undertaken in Hamilton Harbour, Lake Ontario, using the benthic flume Sea Carousel. The measurements were made on a site of low-density, homogeneous natural mud (C) and on two sites artificially disrupted through ploughing. One disrupted site was injected with water (W), the second with a strong oxidant (OIP), calcium nitrate. The results from the three sites were compared to determine the effects of ploughing, bed fluidization and chemical amendment against measures made in marine settings. Several conclusions can be drawn from this study.

(1) The control (undisturbed) erosion thresholds showed a range of values ($0{\cdot}27 < \tau_c(0) < 0{\cdot}5$ Pa) that were similar to marine counterparts of similar bulk density (950–1500 kg^{-3}). Surface buoyant biofilms, similar to those described by Sutherland *et al.* (1998b), were found in the topmost 2 mm of the bed and appear to contribute $\approx 70\%$ of the mean force required for bed erosion.

(2) The erosion thresholds of the (freshwater) sites appeared to fall within the scatter of a linear relationship $\tau_c(0) = 5{\cdot}85 \times 10^{-4}(\rho_b) - 0{\cdot}37$ Pa, which is largely derived from estuarine settings. This suggests that salinity plays no direct role in controlling this index of sediment erodibility.

(3) Mass settling (expressed as a decay constant k, s^{-1}) after induced bed erosion showed a strong linear correlation with peak sediment concentration S_{max}, which is similar to four other examples from marine settings. The inference is that flocculation of freshly eroded aggregates (such as were found within the Sea Carousel during these tests) does not take place, and that settling is dominated by the primary size and density of the eroded aggregates.

(4) The aggregate size determined from still water mass settling at the end of each erosion test showed no differences between the control and the water- and oxidant-injected sites. Mass settling rates were within those of marine counterparts and yielded normal size spectra and median sedimentation diameters in the very fine sand size to coarse silt classes. The median sedimentation diameter (d_s) falls midway between the median diameter measured by the Malvern 2600C and the Optimax V. Systematic trends in aggregate size with flow speed were not evident.

(5) The effect of ploughing of the lakebed was short lived. The bed strength recovered linearly with time ($\tau_c(0,t) = 0{\cdot}16 + 0{\cdot}076(\Delta t)$) to the mean value of the control site (0·34 Pa) in 2·4 days. Consolidation (expressed in terms of the friction coefficient, ϕ) showed trends of fluidization during ploughing ($\phi = 0$) and linear recovery with time ($\phi(0{\cdot}01,t) = 2{\cdot}12(\Delta t)$). The predicted time interval needed for a return to natural conditions ($\phi = 12°$) was 6 days, which is also the time required for full oxidation to take place.

(6) Bedload transport of aggregates began at the onset of bed erosion. Aggregates 2–4 mm in

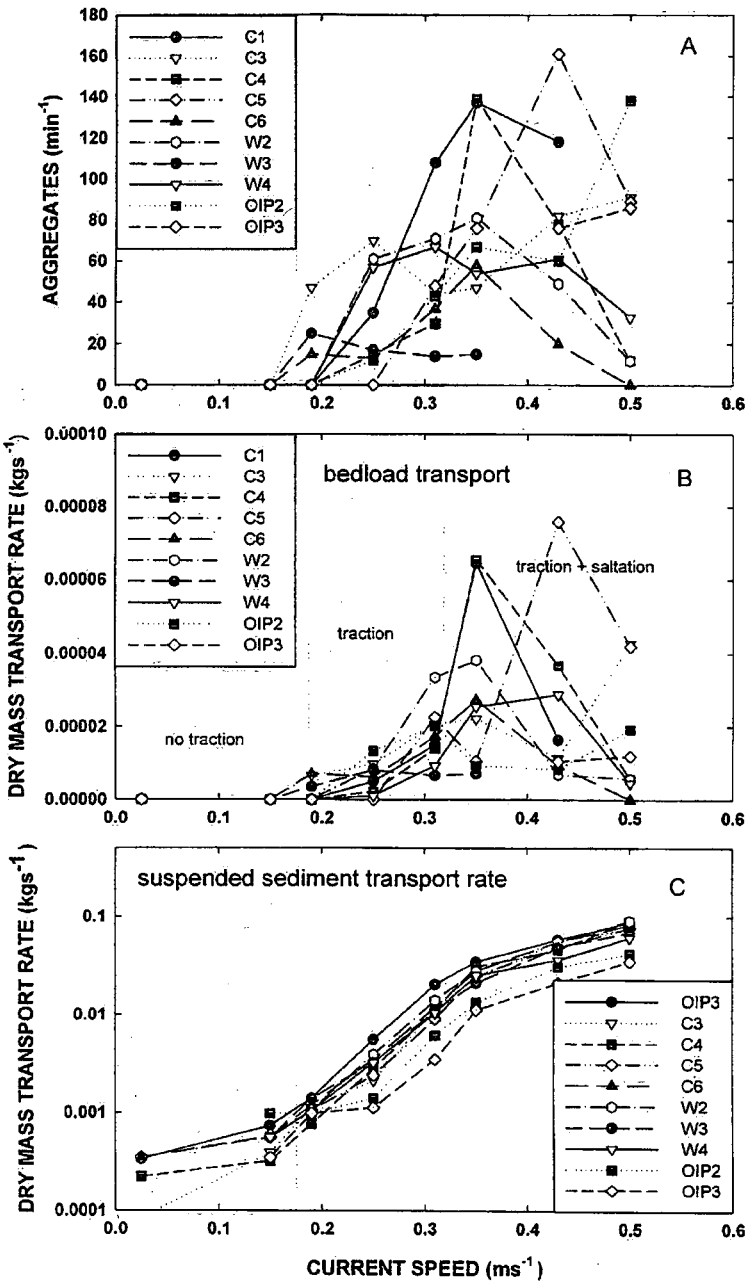

Fig. 10. High-resolution video observations of the size, flux and transport mode of aggregates near the bed throughout the erosion process: (A) aggregate flux (min^{-1}) as a function of current speed (U_y); bedload is seen to be greatest for $U_y = 0{\cdot}4$ ms^{-1} and decreases as the flow approaches the suspension threshold. The diameter of aggregates was between 2 and 4 mm and appeared not to change with flow speed; (B) dry mass transport rate of aggregates as bedload vs. current speed; note the transition from traction to saltation at $U_y = 0{\cdot}35$ ms^{-1}; and (C) the dry mass transport rate of material in suspension as a function of current speed. Notice the similarity in results from all sites and the onset of full aggregate suspension at an extrapolated $U_y = 0{\cdot}6$ ms^{-1}.

diameter moved by surface creep and then in saltation. The bedload flux never exceeded 1% of the suspended flux and decreased throughout the erosion process.

(7) There appears to be no negative long-term impact of remediation on lakebed sediment stability. In later studies, oxidation of sediments using this approach took at least 6–10 days. Thus, future work could measure sediment sulphide concentrations of ambient S as a guide to resuspension by natural events.

ACKNOWLEDGEMENTS

If this project is considered a success, it is due largely to the efforts of several key people. In particular, we wish to thank: A. Robertson who helped mobilize and ship the GSCA Sediment Geodynamics container to Burlington; R. Murphy (GSCA) for technical support to C.L.A. throughout the survey period; H. Don (NWRI) for boat handling and general field logistics while on site in Hamilton Harbour; Dr B. Krishnappan (NWRI)

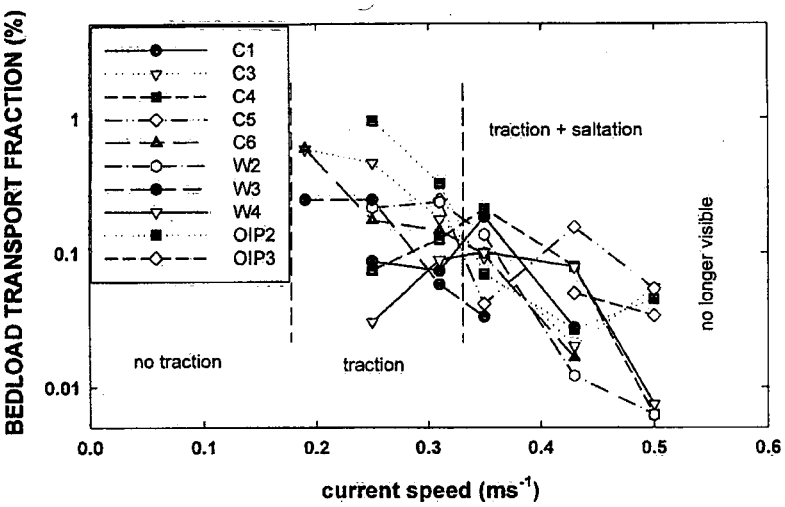

Fig. 11. The ratio of bedload flux to suspended flux as a function of flow speed for all experiments. Notice that the bedload contribution is greatest at the onset of erosion and decreases thereafter. It is no greater than 1% of the suspended flux and thus contributes very little to the sediment mass balance.

for provision of the settling chamber and microscope used in the particle settling analyses; C. Jaskot for analyses of suspended sediments for IGD; and D. Clattenburg (GSCA) for the detailed grain-size analyses. This project was funded by Environment Canada and by RODAC funds to C.L.A. Finally, thanks go to Professor J. L. Best and two anonymous reviewers who significantly improved this manuscript.

NOMENCLATURE

b	Sea Carousel duct width (m)
C_d	drag coefficient
D	net bed mass deposition (kg)
d_{50}	median diameter of disaggregated particles (m)
d_s	sedimentation diameter of aggregates (m)
E	net bed mass erosion (kg)
E_f	floc. erosion rate (kg m^{-2} s^{-1})
E_m	mean bed erosion rate (kg m^{-2} s^{-1})
E_p	peak erosion rate under type I erosion (kg m^{-2} s^{-1})
F_l	lift force at bed due to buoyancy (Pa)
h	eroded depth (m)
h_s	depth of measurement of S
H	Sea Carousel duct height (m)
k	settling decay constant
M	dry mass of sediment in suspension with Sea Carousel (kg)
P	sediment bed porosity
P'	sediment porewater pressure (Pam^{-2})
R	radial speed of Sea Carousel lid (ms^{-1})
S	suspended sediment concentration (kg m^{-3})
S_{max}	maximum suspended sediment concentration at onset of settling (kg m^{-3})
S_o	ambient nearbed suspended sediment concentration (kg m^{-3})
t	time (s)
Δt	time increment in the evaluation of erosion rate (s)
U	azimuthal (tangential) mean current velocity (ms^{-1})
U_y	index tangential velocity measured Sea Carousel (ms^{-1}), where $y = 0{\cdot}18$ m
U^*	friction velocity (ms^{-1})
U^*_s	turbidity corrected friction velocity (ms^{-1})
V	radial mean current velocity (ms^{-1})
V_l	sample volume (m^3)
V_s	sediment volume (m^3)
V_{sc}	Sea Carousel flume volume ($0{\cdot}218$ m^3)
w	Sea Carousel flume width (m)
W	vertical mean current velocity (ms^{-1})
W_s	sediment mass settling rate (ms^{-1})
W_g	suspended sediment weight (kg)
x	azimuthal (tangential) distance (m)
Δy	spatial scale in Sverdrup equation (m)
y	radial distance (m)
z	vertical distance (m)
α	Sea Carousel bed area (m^2)
ρ	ambient seawater density ($k.m^{-3}$)
ρ_s	sediment density (2650 kg^{-3})
ρ_o	clear-water density (kg m^{-3})
ρ_b	sediment bulk density (kg m^{-3})
τ_o	fluid-transmitted bed shear stress (Pa)
$\tau_c(z)$	critical erosion threshold stress at depth z (Pa)
τ_b	sediment yield strength (Pa)
μ	absolute fluid viscosity (m^2 s)
σ'	sediment effective stress (Pa)
ε	diffusion coefficient in the Sverdrup equation
ϕ	internal friction coefficient (degrees)

REFERENCES

Amos, C.L. and **Droppo, I.** (1996) The stability of remediated lakebed sediment, Hamilton harbour, Lake Ontario, Canada. *Geol. Surv. Can. Open File Report*, **2276**, 48 pp.

Amos, C.L. and **Gibson, J.** (1994) The stability of dredge material at dumpsite B, Miramichi Bay, New Brunswick, Canada. *Geol. Surv. Can. Open File Report*, **3020**, 51 pp.

Amos, C.L., Grant, J., Daborn, G. and **Black, K.** (1992) Sea Carousel – a benthic annular flume. *Estuar. Coast. Shelf Sci.*, **34**, 557–577.

Amos, C.L., Sutherland, T.F., Radzijewski, B. and **Doucette, M.** (1996a) A rapid technique to determine bulk density of fine-grained sediments by x-ray computed tomography. *J. Sed. Res.*, **66**, 1023–1025.

Amos, C.L., Sutherland, T.F. and **Zevenhuizen, J.** (1996b) The stability of sublittoral, fine-grained sediments in a subarctic estuary. *Sedimentology*, **43**, 1–19.

Amos, C.L., Feeney, T., Sutherland, T.F. and **Luternauer, J.L.** (1997) The stability and erodibility of fine-grained sediments. *Estuar. Coast. Shelf Sci.*, **45**, 507–524.

Amos, C.L., Brylinsky, M., Sutherland, T.F., O'Brien, D., Lee, S. and **Cramp, A.** (1998a) The stability of a mudflat in the Humber estuary, South Yorkshire, UK. In: *Sedimentary Processes in the Intertidal Zone* (Eds K.S. Black, D.M. Paterson and A. Cramp), *Geol. Soc. London Spec. Publ.*, 139, 25–43.

Amos, C.L., Cloutier, D., Cristante, S., Cappucci, S. and **Levy, A.** (1998b) The Venice Lagoon study (F-ECTS), field results – August, 1998. *Geol. Surv. Can. Open File Report*, **3711**, 31 pp + appendixes.

Amos, C.L., Cloutier, D., Cristante, S. and **Cappucci, S.** (2000) The Venice Lagoon Study (F-ECTS). Field results – February, 1999. *Geol. Surv. Can. Open File Report*, **3904**, 47 pp + appendixes.

Baas, J.H. and **Best, J.L.** (2002) Turbulence modulation in clay-rich sediment-ladened flows and some implications for sediment deposition. *J. Sed. Res.*, **72**, 336–340.

Bagnold, R.A. (1936) *The Physics of Blown Sand and Desert Dunes*. Chapman & Hall, London, 265 pp.

Bagnold, R.A. (1966) An approach to the sediment transport problem from general physics. *US Geol. Surv. Prof. Paper*, **4421**, 37 pp.

Berlamont, J., Ockenden, M., Toorman, E. and **Winterwerp, J.** (1993) The character of cohesive sediment properties. *Coast. Eng.*, **21**, 105–128.

Best, J.L. and **Leeder, M.R.** (1993) Drag reduction in turbulent muddy seawater flows and some sedimentary consequences. *Sedimentology*, **40**, 1129–1137.

Cappucci, S. (2002) *The Stability and Evolution of an Intertidal Mudflat in Venice Lagoon, Italy*. Unpubl. PhD Thesis, University of Southampton, 132 pp + appendixes.

Cardenas, M., Gailani, J., Ziegler, C.K. and **Lick, W.** (1995) Sediment transport in the Lower Saginaw River. *Mar. Freshwater. Res.*, **46**, 337–347.

Crapper, M. and **Ali, K.H.M.** (1997) A laboratory study of cohesive sediment transport. In: *Cohesive Sediments* (Eds N. Burt, R. Parker and J. Watts), pp. 197–211. John Wiley & Sons, Chicester.

Downing, J.P. (1983) An optical instrument for monitoring suspended particulates in ocean and laboratory. *Proceedings of Oceans'83*, pp. 199–202.

Droppo, I.G. and **Amos, C.L.** (2001) Structure, stability, and transformation of contaminated lacustrine surface fine-grained laminae. *J. Sed. Res.*, **71**, 718–727.

Droppo, I.G., Leppard, G.G., Flannigan, D.T. and **Liss, S.N.** (1997) The freshwater floc: a function relationship of water and organic and inorganic floc constituents affecting suspended sediment properties. *Water Air. Soil. Poll.*, **99**, 43–53.

Einstein, H.A. and **Krone, R.B.** (1967) Experiments to determine modes of cohesive sediment transport in salt water. *J. Geophys. Res.*, **67**, 1451–1461.

Fennessy, M.J., Dyer, K.R., Huntley, D.A. and **Bale, A.J.** (1997) Estimation of settling flux spectra in estuaries using INSSEV. In: *Cohesive Sediments* (Eds N. Burt, R. Parker and J. Watts), pp. 87–104. John Wiley & Sons, Chicester.

Gibbs, R.J., Matthews, M.D. and **Link, D.A.** (1971) The relationship between sphere size and settling velocity. *J. Sed. Petrol.*, **41**, 7–18.

Gularte, R.C., Kelly, W.E. and **Nacci, V.A.** (1980) Erosion of cohesive sediments as a rate process. *Ocean Eng.*, **7**, 539–551.

Gust, G. (1976) Observations on turbulent-drag reduction in a dilute suspension of clay in sea-water. *J. Fluid Mech.*, **75**, 29–47.

Gust, G. and **Muller, V.** (1997) Interfacial hydrodynamics and entrainment functions of currently used erosion devices. In: *Cohesive Sediments* (Eds N. Burt, R. Parker and J. Watts), pp. 149–174. John Wiley & Sons, Chicester.

Houwing, E.J. (1999) Determination of the critical erosion threshold of cohesive sediments on the intertidal mudflats along the Dutch Wadden Sea coast. *Estuar. Coast. Shelf Sci.*, **49**, 545–555.

Irvine, K.N., Droppo, I.G., Murphy, T.P. and **Stirrup, D.M.** (1998) Annual loading estimates of selected metals and PAHs in CSOs, Hamilton, Ontario using a continuous PCSWMM approach. In: *Advances in Modeling the Management of Stormwater Impacts*, Vol. 6 (Ed. W. James), pp. 383–398. Annarbor Press.

Krone, R.B. (1962) *Flume Studies of the Transport of Sediment in Estuarial Shoaling Processes*. Final Report Hydraulic Engineering Laboratory and Sanitary Engineering Research Laboratory. University of California, Berkeley, CA.

Lau, Y.L. and **Krishnappan, B.G.** (1994) Does reentrainment occur during cohesive sediment settling? *J. Hydraul. Res.*, **120**, 236–244.

Lavelle, J.W. and **Mofjeld, H.O.** (1985) Do critical stresses for incipient motion and erosion really exist? *J. Hydraul. Res.*, **113**, 370–393.

Lavelle, J.W., Mofjeld, H.O. and **Baker, E.T.** (1984) An in situ erosion rate for a fine-grained marine sediment. *J. Geophys. Res.*, **89**, 6543–6552.

Lee, D.-Y., Lick, W. and **Kang, S.W.** (1981) The entrainment and deposition of fine-grained sediments in Lake Erie. *J. Great Lakes Res.*, **7**, 224–233.

Li, M.Z. and **Gust, G.** (2000) Boundary layer dynamics and drag reduction in flows of high cohesive sediment suspensions. *Sedimentology*, **47**, 71–86.

Lick, W., Lick, J. and **Zeigler, C.K.** (1992) Flocculation and its effect on the vertical transport of fine-grained sediments. *Hydrobiologia*, **235/236**, 1–16.

Lick, W., Lick, J. and **Zeigler, C.K.** (1994) The resuspension and transport of fine-grained sediments in Lake Erie. *J. Great Lakes Res.*, **20**, 599–612.

Liss, S.N., Droppo, I.G., Flannigan, D. and **Leppard, G.G.** (1996) Floc architecture in wastewater and natural riverine systems. *Environ. Sci. Technol.*, **30**, 680–686.

McDowell, D.M. and **O'Connor, B.A.** (1977) *Hydraulic Behaviour in Estuaries*. MacMillan Press, London, 292 pp.

Middleton, G.V. and **Southard, J.B.** (1984) Mechanics of Sediment Movement. *SEPM Short Course*, **3**, 401 pp.

Mitchener, H. and **Torfs, H.** (1996) Erosion of mud/sand mixtures. *Coast. Eng.*, **29**, 1–25.

Murdoch, A. and **Zeman, A.J.** (1975) Physicochemical properties of dredge spoil. *J. Waterw. Port Coast. Ocean Eng.*, **101**, 201–216.

Murphy, T.P., Moller, A. and **Brouwer, H.** (1995) *In situ* treatment of Hamilton Harbour sediment. *J. Aquat. Ecosyst. Health*, **4**, 195–203.

Murphy, T.P., Moller, A., Pandey, R., Brouwer, H., Fox, M., Babin, J. and **Gray, K.** (1996) St Mary's River – chemical treatment of contaminated sediments by iron injection. In: *Ecosystem Ecology: Ecology, Fisheries and Management* (Eds M. Munawar, T. Edsall and J. Leach), pp. 397–412. Academic Press, New York.

Parchure, T.M. and **Mehta, A.J.** (1985) Erosion of soft cohesive sediment deposits. *J. Hydraul. Eng.*, **111**, 1308–1326.

Parsons, T.R., Maita, Y. and **Lalli, C.M.** (1984) *A Manual of Chemical and Biological Methods for Seawater Analysis*, pp. 107–110. Pergamon Press, Oxford.

Partheniades, E., Cross, R.H. and **Ayora, A.** (1968) Further results on the deposition of cohesive sediments. In: *Proceedings 11th Conference on Coastal Engineering*, London, pp. 723–742.

Paterson, D.M. (1989) Short-term changes in the erodibility of intertidal cohesive sediments related to the migratory behaviour of epipelic diatoms. *Limnol. Oceanogr.*, **34**, 223–234.

Rukavina, N.A. and **Versteeg, J.G.** (1996) Surficial sediments of Hamilton Harbour: physical properties and basin morphology. *Water Quality Res. J. Can.*, **31**, 529–551.

Sutherland, T.F. (1996) Biostabilization of Estuarine Subtidal Sediments. Unpubl. PhD Thesis, Dalhousie University, Halifax, 179 pp.

Sutherland, T.F., Amos, C.L. and **Grant, J.** (1998a) The erosion threshold of biotic sediments: a comparison of methods. In: *Sedimentary Processes in the Intertidal Zone* (Eds K.S. Black, D.M. Paterson and A. Cramp), *Geol. Soc. London Spec. Publ.*, 139, 295–307.

Sutherland, T.F., Amos, C.L. and **Grant, J.** (1998b) The effect of buoyant biofilms on the erodibility of sublittoral sediments of a temperate microtidal estuary. *Limnol. Oceanogr.*, **43**, 225–235.

Sverdrup, H.U. (1952) *Oceanography for Meteorologists*. George Allen & Unwin, London, 246 pp.

Terzaghi, K. and **Peck, R.B.** (1967) *Soil Mechanics in Engineering Practice*. John Wiley & Sons, New York, 729 pp.

Thompson, C.E.L., Amos, C.L., Jones, T.E.R. and **Chaplin, J.** (2003) The manifestation of fluid-transmitted bed shear stress in a smooth annular flume – a comparison of methods. *J. Coast. Res.*, (in press).

Tolhurst, T.J., Riethmuller, R. and **Paterson, D.M.** (1997) In situ versus laboratory analysis of sediment stability from intertidal mudflats. *Cont. Shelf Res.*, **20**, 1317–1334.

Villaret, C. and **Paulic, M.** (1986) *Experiments on the Erosion of Deposited and Placed Cohesive Sediments in an Annular Flume*. Report to Coastal and Oceanographic. Engineering Department, University of Florida, Gainesville.

Williamson, H.J. and **Ockenden, M.C.** (1996) ISIS: an instrument for measuring erosion shear stress in situ. *Estuar. Coast. Shelf Sci.*, **42**, 1–18.

Ziegler, C.K. and **Lick, W.** (1997) Numerical modelling of the transport and fate of hydrophobic contaminants and fine-grained sediments in surface waters. In: *Next Generation Environmental Models and Computational Methods* (Eds G. Delic and M.F. Wheeler), pp. 129–138. SIAM, Philadelphia.

Ziegler, C.K. and **Nisbet, B.** (1994) Fine-grained sediment transport in Pawtuxest River, Rhode Island. *J. Hydraul Eng.*, **120**, 561–575.

Ziegler, C.K. and **Nisbet, B.S.** (1995) Long-term simulation of fine-grained sediment transport in large reservoirs. *J. Hydraul. Eng.*, **121**, 773–781.

Manuscript received 8 November 2001; revision accepted 2 October 2002.